Mon. Not. R. Astron. Soc. **397,** 1728–1738 (2009) doi:10.1111/j.1365-2966.2009.15040.x

The link between SCUBA and *Spitzer*: cold galaxies at $z \lesssim 1$

M. Symeonidis,[1⋆] M. J. Page,[1] N. Seymour,[1] T. Dwelly,[2] K. Coppin,[3] I. McHardy,[2] G. H. Rieke[4] and M. Huynh[5]

[1]*University College London, Mullard Space Science Laboratory, Holmbury St. Mary, Dorking, Surrey RH5 6NT*
[2]*School of Physics & Astronomy, University of Southampton, Southampton, Hampshire SO17 1BJ*
[3]*Institute for Computational Cosmology, Durham University, South Road, Durham DH1 3LE*
[4]*Department of Astronomy, The University of Arizona, Tucson, AZ 85721, USA*
[5]*Spitzer Science Center, California Institute of Technology, 1200 East California Boulevard, Pasadena, CA 91125, USA*

Accepted 2009 May 6. Received 2009 May 5; in original form 2009 March 21

ABSTRACT

We show that the far-IR properties of distant Luminous and UltraLuminous InfraRed Galaxies (LIRGs and ULIRGs, respectively) are on average divergent from analogous sources in the local Universe. Our analysis is based on *Spitzer* Multiband Imaging Photometer (MIPS) and Infrared Array Camera (IRAC) data of $L_{\rm IR} > 10^{10}\,{\rm L}_{\odot}$, 70 μm selected objects in the $0.1 < z < 2$ redshift range and supported by a comparison with the *IRAS* Bright Galaxy Sample. The majority of the objects in our sample are described by spectral energy distributions (SEDs) which peak at longer wavelengths than local sources of equivalent total infrared luminosity. This shift in SED peak wavelength implies a noticeable change in the dust and/or star-forming properties from $z \sim 0$ to the early Universe, tending towards lower dust temperatures, indicative of strong evolution in the cold dust, 'cirrus', component. We show that these objects are potentially the missing link between the well-studied local IR-luminous galaxies, *Spitzer* IR populations and SCUBA sources – the $z < 1$ counterparts of the cold $z > 1$ SubMillimetre Galaxies (SMGs) discovered in blank-field submillimetre surveys. The *Herschel Space Observatory* is well placed to fully characterize the nature of these objects, as its coverage extends over a major part of the far-IR/sub-mm SED for a wide redshift range.

Key words: galaxies: general – galaxies: high-redshift – galaxies: photometry – galaxies: starburst – infrared: galaxies.

1 INTRODUCTION

In the past 30 years, the field of infrared astronomy has instigated immense breakthroughs in our understanding of the cosmos, at the same time driving pioneering technological advances (see review by Low, Rieke & Gehrz 2007). Discovering and resolving a large part of the Cosmic InfraRed Background (CIRB) (Stanev & Franceschini 1998; Gorjian, Wright & Chary 1999) led to valuable insights on the nature of the sources that are responsible for more than half of the cosmic electromagnetic energy density originating from star formation and Active Galactic Nuclei (AGN). Only one-third of the CIRB is attributed to the local galaxies discovered in abundance by the *InfraRed Astronomical Satellite* (*IRAS*), which implies that a major part of it is composed of redshifted infrared light originating from galaxies at high redshift. Moreover, the CIRB intensity and peak wavelength suggest that the main contributors are dust-obscured populations whose bolometric energy output is dominated by emission in the infrared. As studies have repeatedly confirmed, these galaxies hide an immensely active interstellar medium (ISM), they are the ultimate stellar nurseries, many also hosting deeply embedded and rapidly growing AGN (e.g. Soifer et al. 1986; Sanders et al. 1987; Genzel et al. 1998; Tacconi et al. 2002).

Following these discoveries, a classification scheme was introduced based on the total infrared luminosity ($L_{\rm IR}$) in the 8–1000 μm spectral region, and four main classes of IR-luminous galaxies were defined: starbursts (SBs; $10^{10} < L_{\rm IR} < 10^{11}\,{\rm L}_{\odot}$), Luminous InfraRed Galaxies (LIRGs; $10^{11} < L_{\rm IR} < 10^{12}\,{\rm L}_{\odot}$), UltraLuminous InfraRed Galaxies (ULIRGs; $10^{12} < L_{\rm IR} < 10^{13}\,{\rm L}_{\odot}$) and HyperLuminous InfraRed Galaxies (HyLIRGs; $L_{\rm IR} > 10^{13}\,{\rm L}_{\odot}$) (e.g. Sanders & Mirabel 1996; Genzel et al. 1998). This classification is non-arbitrary and a good representation of the generic characteristics of these sources, since the transition in energetic output from 10^{10} to $10^{14}\,{\rm L}_{\odot}$ is a consequence of a change in dust properties, star formation history (e.g. Brinchmann & Ellis 2000; Cole et al. 2000), stellar mass (e.g. Bundy et al. 2006), morphology (e.g. Murphy et al. 1996; Wang et al. 2006) and the role of the central black hole (e.g. Veilleux, Sanders & Kim 1997; Brand et al. 2006).

⋆E-mail: msy@mssl.ucl.ac.uk

With data from *Spitzer*, doors to the high-redshift Universe were opened, in terms of both resolving the CIRB (e.g. Lagache, Puget & Dole 2005; Dole et al. 2006) and accurately pinpointing the evolution of the infrared luminosity function (e.g. Le Floc'h et al. 2005; Huynh et al. 2007a), as well as identifying the key processes responsible for the extreme luminosities of these galaxies (e.g. Franceschini et al. 2003). In terms of extragalactic science and specifically deep *Spitzer* surveys, the capabilities of Multiband Imaging Photometer for *Spitzer* (MIPS) have been extensively exploited in the mid-IR, enabling the nature of the 24 μm population to be characterized up to $z \sim 3$ (e.g. Chary et al. 2004; Marleau et al. 2004; Le Floc'h et al. 2004, 2005; Houck et al. 2005; Dole et al. 2006; Marcillac et al. 2006). Work on the 160 μm population has been limited to source count analysis (Dole et al. 2004; Frayer et al. 2006a), whereas 70 μm selected sources have also been characterized with respect to their IR colours, mid-IR spectra and the infrared luminosity function (Dole et al. 2004; Frayer et al. 2006a,b; Huynh et al. 2007a; Brand et al. 2008).

The difference in resolution and sensitivity between the three MIPS bands has not enabled a true unification of 24, 70 and 160 μm populations and hence the range and types of galaxies that dominate each one. For example, all *Spitzer* sources detected at 70 μm have 24 μm counterparts, but the reverse is not true, as the sensitivity of MIPS at 24 μm is up to a factor of 100 higher than at 70 μm, considerably greater than the f_{70}/f_{24} flux density ratio for the average IR-luminous galaxy at $z > 1$ (typically <30; Papovich et al. 2007). In addition, there is a wide range of sources with weak far-IR emission that would form part of a 24 μm survey, but would not necessarily have detections in the MIPS 70 or 160 μm bands, such as quiescently star-forming spirals, low-redshift early-type galaxies, optically selected quasars and obscured AGN (e.g. Yan et al. 2004; Desai et al. 2008). On the contrary, due to the lower sensitivity of MIPS at 70 μm, the majority of far-IR-selected objects conform to one main type and are thus defined by large amounts of dust, high IR-to-optical ratios and high star formation rates (SFRs); they are predominantly SBs, LIRGs and ULIRGs (Symeonidis et al. 2007, 2008, hereafter S08). This brings a high degree of homogeneity in the 70 μm population, clearly benefiting any study of its evolution with redshift.

Infrared spectral energy distributions (SEDs) for *Spitzer*-selected sources have been examined with and without individual 70 and 160 μm detections, the latter via 70 and 160 μm stacking on the 24 μm positions (Papovich et al. 2007; Zheng et al. 2007; Bavouzet et al. 2008) and the former with data from various surveys, such as the *Spitzer* Infrared Nearby Galaxies Survey (SINGS) (Kennicutt et al. 2003), the *Spitzer* Wide-area InfraRed Extragalactic survey (SWIRE) (Lonsdale et al. 2003, 2004), the All-wavelength Extended Groth Strip Survey (AEGIS) (Davis et al. 2007), the Bootes field of the NOAO Deep Wide Field Survey (NDWFS) and the *Spitzer* First Look Survey (FLS) (see Dale et al. 2005; Rowan-Robinson et al. 2005; Symeonidis et al. 2007; Bavouzet et al. 2008; S08 for work on SEDs). However, due to *Spitzer*'s limited sensitivity and angular resolution at the long wavelengths, the exact shape of the SED for various galaxy types has not been examined to the detail merited for the high-redshift Universe. For non-local sources, the short wavelength (Wien) side of the SED peak has been mapped in the mid-IR and far-IR up to $z \sim 2$ and ∼1, respectively, whereas sub-mm studies have examined the long wavelength (Rayleigh–Jeans) side up to $z \sim 3$. Although it seems that cumulative data over such a wide wavelength and redshift range would have enabled the complete characterization of the IR SED, the different sensitivities of mid-IR, far-IR and sub-mm surveys do not favour homogeneous investigations, and as a result many details on the SED are missing. Moreover, these 'bolometric' studies do not provide detailed information on the key intragalactic environments which dominate the energy budget, and as a result, fundamental questions with respect to the evolution of the properties of obscured galaxies still remain unanswered.

The natural question that follows is whether local infrared galaxies are the same, similar for the most part or instead very different from their high-redshift counterparts. Here, we approach this topic by comparing the SEDs of local ($z \sim 0$) infrared galaxies with galaxies at $z > 0.1$, selected at 70 μm, based on the preliminary results of S08. In Section 2, we define the sample and outline the various selection criteria. Sections 3 and 4 form the main body of our analysis, where we describe our methodology and results, paying particular attention to any biases that could have been introduced. In Section 5, we discuss the implication of our results, making comparisons to other studies. Finally, the summary and conclusions are presented in Section 6. Throughout, we use a concordance model of Universe expansion, $H_0 = 70\ \mathrm{km\,s^{-1}\,Mpc^{-1}}$, $\Omega_\mathrm{M} = 0.3$ and $\Omega_\Lambda = 0.7$ (Spergel et al. 2003).

2 SAMPLE SELECTION

This work is based on Guaranteed Time Observations (GTO) using the MIPS (Rieke et al. 2004) on the *Spitzer Space Telescope* (Werner et al. 2004) in the Extended Groth Strip (EGS) field (∼0.5 deg^2) (Davis et al. 2007) and 13^H *XMM–Newton*/*Chandra* Deep Field (∼0.6 deg^2, centred on $13^\mathrm{h}34^\mathrm{m}37^\mathrm{s}+37^\circ54'44''$; Seymour et al. 2008). We select the sample at 70 μm and retrieve 178 objects down to ∼4 mJy (5σ) in the EGS and 244 objects down to ∼8 mJy (5σ) in 13^H Field. As these two surveys cover similar areas and share a similar photometric completeness limit at $f_{70} \sim 10$ mJy, we are able to combine the data into one congruous sample, where $4 < f_{70} < 290$ mJy.

2.1 Source extraction and photometric coverage

For details on MIPS data reduction and source extraction, we refer the reader to Symeonidis et al. (2007) and Seymour et al. (2009), for the EGS and the 13^H field, respectively. Each 70 μm object was matched to the brightest 24 μm source within 8 arcsec, in accordance with the MIPS PSF. Given the relative sensitivity limits (∼110 μJy for 24 μm and ∼10 mJy for 70 μm), two sources near the 70 μm 5σ flux density limit with no 24 μm counterparts were considered spurious and discarded. The 160 μm photometry was extracted with the IRAF/DIGIPHOT package on the known positions of the 70 μm sources, enabling us to go nearer the confusion limit, estimated to be of the order of ∼40 mJy at 160 μm (e.g. Dole, Lagache & Puget 2003). We used an aperture radius of 40 arcsec (equivalent to the 160 μm diffraction limit) and the aperture corrections specified by the MIPS team (1.884 for a 40 arcsec radius and 40–75 arcsec background annulus; http://ssc.spitzer.caltech.edu/mips/apercorr/). We tested our method of source extraction on the Spitzer Cosmic Evolution Survey (S-COSMOS; Frayer et al. 2009) 160 μm image, with the known positions of the S-COSMOS 160 μm sources and found our flux density estimates to be consistent, within 10 per cent (rms) of the S-COSMOS MOPEX (Makovoz & Marleau 2005) estimates.

The MIPS photometry was supplemented with Infrared Array Camera (IRAC) 8 μm data to ensure a more extensive coverage of the infrared SED. The overlapping area of the 8, 24 and 160 μm images adds up to about 65 per cent of the EGS 70 μm survey and 54 per cent of the 13^H field 70 μm survey. Requiring IRAC coverage

results in a subset of 114 70 μm sources in the EGS and 132 in the 13^H field, instead of the 178+224 described earlier.

2.2 Redshifts for the 13^H field

Photometric redshifts were estimated for the 13^H field, using multi-band deep optical and near-IR imaging: $u^*, B, g', R, i', I, z', Z, J, H$ and K, from various ground-based observatories [Canada–France–Hawaii Telescope (CFHT), Subaru, Isaac Newton Telescope (INT) and United Kingdom Infrared Telescope (UKIRT)] and 3.6, 4.5, 5.8, 8.0 μm from *Spitzer*'s IRAC. The requirement of area coverage in at least four optical/near-IR bands reduced the number of available 70 μm sources from 132 to 108. The cross-matching was done using the 24 μm positions each 70 μm source was identified with. Photometric redshifts were estimated with the HyperZ (Bolzonella, Miralles & Pelló 2000) template fitting code, including the set of galaxy and AGN SED templates from Rowan-Robinson et al. (2008) and setting optical extinction as a free variable. All aperture magnitudes were also corrected for aperture losses. Moderate optical extinction was permitted for the AGN and late-type galaxy templates, and heavy extinction (up to $A_V = 10$) was allowed for the SB templates. For a full description of the photometry extraction and redshift fitting process, see Dwelly et al. (in preparation).

Within the final overlap area of the *Spitzer* MIPS/IRAC and ground-based optical/near-IR surveys, 39 good-quality spectroscopic redshifts are also available, as part of an ongoing program to identify the optical counterparts of faint X-ray and radio sources in the 13^H field, using various long-slit and multi-object spectrographs at the William Herschel Telescope (WHT), CFHT and Keck telescopes. The reliability of the photometric redshifts was checked against the spectroscopic redshifts, finding high consistency with an rms scatter in redshift of only ∼0.05.

Finally, as the aim of this work is to evaluate the properties of non-local 70 μm selected sources, we made a redshift cut at $z = 0.1$, rejecting the 26 low-redshift resolved bright galaxies in the 13^H field. The final 13^H field redshift sample consists of 82 sources, 34 with spectroscopic redshifts and 48 with photometric redshifts.

2.3 Redshifts for the EGS

Spectroscopic redshifts for the EGS were acquired by the Deep Extragalactic Evolutionary Probe 2 (DEEP 2) survey (Davis et al. 2003). DEEP 2 targeted sources in the EGS with a magnitude limit of $R_{AB} = 24.1$. The brightest, most extended sources were weeded out of the spectroscopic targeting algorithms, as their photometry was suspect and they could potentially saturate the detector. Thereafter, the retrieval of redshifts was random, at ∼60 per cent sampling and at the time of writing there were 66 good-quality redshifts available for the 114 sources in the MIPS/IRAC overlap areas. These are in the range $0.1 < z < 1.9$, with a mean of 0.55 and a median of 0.48. The exclusion of the brightest $R < 18$ sources implies that there is an under-representation of extended, low-redshift galaxies. However, as we apply a redshift cut at $z = 0.1$ (see Section 2.2), these would have been eliminated from our final sample anyway. On the faint end, there are only four objects fainter than $R = 24.1$ in the full sample, i.e. only two would have made it in the redshift sample, so overall there is high consistency between the two samples.

The limited optical photometry for the EGS 70 μm objects did not allow us to calculate reliable photometric redshifts, and as a result, we only use these 66 sources with spectroscopic redshifts in subsequent work. However, as outlined above, this redshift sample is a good representation of the $z > 0.1$ parent EGS sample.

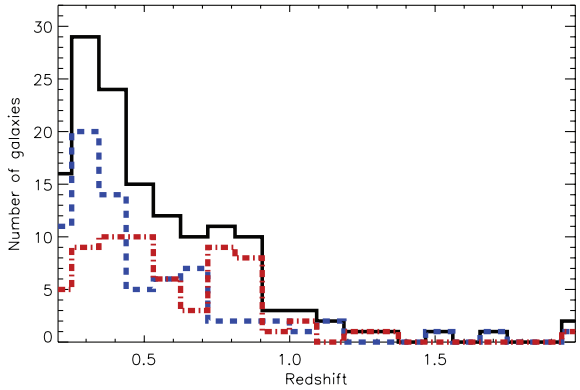

Figure 1. The combined redshift distribution of the *70 μm sample* ($z_{\rm mean} \sim 0.5$, $z_{\rm median} \sim 0.42$; solid black line) from the individual distributions of the EGS population (dot–dashed red line) and the 13^H field population (dashed blue line). The difference between the two redshift distributions is likely due to sample variance.

2.4 The final 70 μm sample

All 148 sources, assembled after the various area and redshift cuts described in earlier sections, are detected at 8 and 24 μm. Eight sources have signal-to-noise ratio of <1 at 160 μm and are therefore excluded from subsequent analysis. From the remaining 160 μm measurements, ∼80 per cent are $>3\sigma$ detections, ∼62 per cent $>5\sigma$ and ∼47 per cent $>7\sigma$.

The final sample consists of 140 galaxies in the 0.1–2 redshift range ($z_{\rm mean} \sim 0.5$, $z_{\rm median} \sim 0.42$, hereafter the *70 μm sample*). Fig. 1 shows the individual and combined redshift distributions, the differences likely arising due to sample variance.

Completeness is not a strict requirement for our analysis, although the selection criteria we apply ensure that the *70 μm sample* is representative of the parent 70 μm population. None the less, given the strong correlation between R-band magnitude and redshift, we examine the possibility that the requirement of (optically derived) redshifts modifies the type of 70 μm sources present in the final sample. We find that the redshift at which each source becomes too faint for inclusion in the 70 μm sample is much lower than the redshift at which it drops out of the R-band survey. This is to be expected as the R-band limit (<1 μJy) is 4–5 orders of magnitude lower than the 70 μm flux density limit (∼10 mJy), but at the same time ∼95 per cent of the objects have $f_{70}/f_R < 5000$. Under these circumstances, sources would drop out of the 70 μm selection before dropping out of the optical selection, confirming that the sample of 140 sources we focus on is representative of $z > 0.1$ 70 μm detected galaxies.

2.5 The local sample

In order to compare local and high-redshift sources in a way that is as unbiased as possible, we evaluate our results against 259 galaxies from the *IRAS* revised Bright Galaxy Sample (BGS) selected at 60 μm (hereafter the *local sample*) by using available photometry from Sanders et al. (2003, hereafter S03). The *IRAS* BGS is particularly suitable for such a comparison because it includes all nearby LIRGS and ULIRGs, and the 60 μm selection criterion is comparable to 70 μm at $z \sim 0.1$ where our sample begins. We do not weed out any sources which potentially have a significant AGN contribution from either the *local* or the *70 μm sample*. Apart from the fact that there is a low AGN incidence in far-IR selected samples, both populations are defined by powerful far-IR emission, hence the

presence of large amounts of dust, explicitly setting star formation to be a very significant part of the galaxies' energetics, if not the dominant. The *IRAS* BGS consists of 629 galaxies ($z \lesssim 0.08$), the majority of which are SBs, but with a significant LIRG population of ∼25 per cent and a very small fraction of ULIRGs (∼2 per cent). We only use galaxies which are not flagged as having large uncertainties in the photometry: all the available LIRGs and ULIRGs (143 and 18) and 98 randomly selected SBs. As our main conclusions rest on the comparison between local and high-redshift LIRGs and ULIRGs and much less so on SBs, we believe it unnecessary to include all of the *IRAS* SBs in the *local sample*. Consequently, we rely on a randomly selected subset, which is about three to four times the number of SBs in the *70 μm sample*, to represent the BGS SBs.

3 SED FITTING

The SED shape of an IR-luminous galaxy in the 5–1000 μm range (rest wavelength) is dominated by emission from dust, with a range of temperatures spanning ∼3 orders of magnitude from ∼1500 K at the shortest wavelengths to ∼10 K at the longest. In the near-IR (∼2–5 μm), light from stellar photospheres dominates the continuum, although there can be a small contribution from dust (e.g. Lu et al. 2003), subsequently becoming negligible shortwards of 2 μm, as the maximum grain sublimation temperature is of the order of ∼1500 K. The mid- to far-IR part of the SED has two major contributions: emission from stochastically heated Very Small Grains (VSGs), with $T > 60$ K, responsible for the continuum up to about $\lambda \sim 40$ μm and emission from large grains in thermal equilibrium, with $T < 50$ K, responsible for emission longwards of $\lambda \sim 40$ μm (e.g. Efstathiou & Rowan-Robinson 1990, 1995; Granato & Danese 1994; Silva et al. 1998; Klaas et al. 2001). Accordingly, the rest-frame SED peak, which defines the wavelength of maximum energetic output (in νf_ν), is in the 40–140 μm range and the SED is often approximated by a modified blackbody ($B_\nu \nu^\beta$) of $T \sim 20$–60 K and emissivity $\beta \sim 1$–2. As the bulk of the dust mass is in equilibrium, such an approximation does represent the average SED shape; however a colder, 'cirrus' component associated with the properties and distribution of dust in the ISM and the intensity of the diffuse radiation field is often missed. If the cold component is significant, yet ignored, the integrated energy output of the galaxy will be underestimated, but more importantly it will lead to erroneous estimates for physical quantities, such as dust mass, emissivity, opacity and temperature (see e.g. Silva et al. 1998, Granato et al. 2000 and Siebenmorgen, Krügel & Laureijs 2001, where the importance of both the SB and cirrus components is emphasized).

In this paper, we broadly categorize the sources as 'cold' or 'warm', depending on the average temperature that defines the bulk of the dust mass, which, as mentioned earlier, is mostly found to be in thermal equilibrium. As a result of the latter, the average dust temperature scales with the inverse of the SED peak wavelength; a cold galaxy SED is expected to peak at longer wavelengths, whereas a warm SED will peak at shorter wavelengths. Note that this is not the same as the classical *IRAS* 'warm/cold' terminology parametrized as the mid-IR f_{25}/f_{60} continuum slope. The *IRAS* 'warm/cold' f_{25}/f_{60} criterion is based on the expectation that dust heated by an AGN would reach higher temperatures and hence lower the continuum slope between 25 and 60 μm (or 24 and 70 μm in *Spitzer*'s case) (e.g. Farrah et al. 2005; Verma et al. 2005; Frayer et al. 2006a); it has been applied extensively in order to quantify relative AGN/SB contributions in ULIRGs (e.g. de Grijp et al. 1985; Miley, Neugebauer & Soifer 1985; Soifer et al. 1989). What we refer to as cold/warm is not related to the mid-IR continuum slope, but solely to the far-IR properties and, more specifically, the position of the SED peak.

3.1 Methodology

We fit the available IR data for the *70 μm* and *local sample* with the Siebenmorgen & Krügel (2007, hereafter SK07) *theoretical* SED templates. In S08, we found that these models are optimum for fitting a wide range of source types, as their formulation employs a configuration of stars and dust distributed throughout the volume. In the SK07 formulation, mid-IR emission originating in dust regions enveloping OB stars is deconvolved from the cirrus emission due to the general stellar radiation field, allowing the far-IR part of the SED to be modelled as a two-temperature component [see also Klaas et al. (2001) and Dunne & Eales (2001) for the benefits of a two-temperature far-IR formulation]. The SK07 library consists of ∼7000 templates defined by the physically acceptable combinations of the following five parameters: radius of dust emitting region (0.35, 1 and 3 kpc), visual extinction ($A_V = 2$–150), total infrared luminosity (10^{10}–$10^{14.7}$ $L_\odot$), hotspot dust density (100–10 000 cm^{-3}) and $L_{\rm stars,OB}/L_{\rm stars,tot}$ (40, 60 and 90 per cent). Hotspot dust density refers to the density of the dust region enveloping OB stars. $L_{\rm stars,OB}/L_{\rm stars,tot}$ represents the percentage of the total infrared luminosity that originates from OB stars, compared to the contribution from the general stellar population.

We perform a χ^2 fit on the photometry (8–160 μm for the *70 μm sample*; 12–100 μm for the *local sample*), using the entire range of SK07 templates, folding in the photometric redshift uncertainties (where applicable). For each object, we determine one interesting parameter, namely the wavelength of the SED (νL_ν) peak, calculated using the mean (and 1σ uncertainty) of all templates with $\chi_i^2 \leq \chi_{\rm min}^2 + 1$, where '$i$' is the template index and $\chi_{\rm min}^2$ is the minimum χ^2 value. In the same way, we also get estimates for the total infrared luminosity ($L_{\rm IR}$, 8–1000 μm) and sub-mm flux density at 350 and 850 μm.

We find that the *70 μm sample* consists of 30 SBs, 79 LIRGs, 29 ULIRGs and three HyLIRGs, indicating that down to the ∼10 mJy level, $L > 10^{10}$ $L_\odot$ sources are the sole contributors to $z > 0.1$ 70 μm populations.

Note that any comparison between IR galaxies at various redshifts will only be fair if each luminosity class is examined separately. As outlined in Section 1, the transition in luminosity closely follows changes in the galaxies' physical properties, star formation history, etc., which must be reflected in all comparative evaluations, something that we maintain throughout this work.

3.2 Selection issues

3.2.1 The SED models and fitting accuracy

We chose the SK07 models, as their theoretical formulation allows the representation of a wide range of systems, minimizing assumptions on the types of sources that exist. This is in contrast to *empirical* sets of templates, e.g. Chary & Elbaz (2001) (hereafter CE01), Dale & Helou (2002), which are tailored to local galaxies and could potentially predispose the results towards the types of SEDs found locally. In S08, we show that this is indeed the case and find them un-representative of the SEDs of 70 μm detected galaxies, especially in the far-IR. In contrast, we find that the SK07 models are representative of the SEDs of both the *local* and *70 μm samples*.

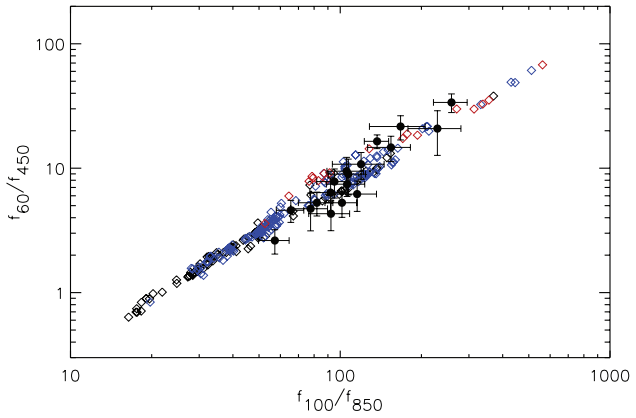

Figure 2. The 60/450 versus 100/850 flux density ratio for local galaxies. Open diamonds: predicted colours for the *local sample* using the SK07 fits (black for SBs, blue for LIRGs and red for ULIRGs). Filled black circles: observations from DE01. Note the good agreement between predicted and observed colours, verifying both the accuracy of our fitting method and the validity of the SK07 models.

To quantify this further, we compare to sub-mm data from Dunne et al. (2000, hereafter D00) and DE01, who describe the sub-mm properties of local galaxies in the SCUBA Local Universe Galaxy Survey (SLUGS) and report 850 and 450 μm observations for a fraction of the local *IRAS* BGS sample. Using the SK07 models, we predict 60, 100, 450 and 850 μm flux densities for the sources in the *local sample* and evaluate the results against the observed Dunne & Eales 2001 (hereafter, DE01) far-IR/sub-mm colours (60/450 versus 100/850, Fig. 2). We find good agreement between our predictions and the DOO DE01 observations, which confirms both the accuracy of our fitting method and the validity of the SK07 templates.

3.2.2 *The detection limits of the 60 μm IRAS survey and 70 μm Spitzer survey*

Selecting the sample at a wavelength shortwards of the peak (the Wien side of the SED), by definition, does not predispose the selection towards cold sources, in the same way that selecting longwards of the peak (the Rayleigh–Jeans side) does not predispose towards warm sources. Our 70 μm selection is well into the Wien side of the SED (for $z > 0.2$, it corresponds to $\lambda_{\rm rest} < 58$ μm), so any bias would favour the selection of warmer SEDs, especially for galaxies at $z > 0.5$. The 60 μm *IRAS* selection probes longer wavelengths in local galaxies than the 70 μm MIPS photometry for sources at $z > 0.2$, so, if anything, it should be more sensitive to relatively cold SEDs. Also note that the 160 μm photometry coincides with the *IRAS* 100 μm band for sources at $0.4 < z < 1$; this applies to all ULIRGs and the higher luminosity LIRGs in the *70 μm sample*.

We estimate the 60 μm flux density the 70 μm sources would have if at the average redshift of the *local sample* ($z \sim 0.012$, ∼50 Mpc) and compare with the f_{60} distribution for the *local sample*, finding considerable overlap (Fig. 3, top panel). It is only the lowest luminosity 70 μm detected SBs ($L < 5 \times 10^{10}\,{\rm L}_{\odot}$) that would not be recovered within the *IRAS* 60 μm flux density limit of 5.24 Jy. This is not surprising, as at 70 μm we detect them at the mJy level and at low redshifts ($z < 0.2$). Using a (conservative) 70 μm 10 mJy flux density limit and the SK07 templates matched to the *IRAS* galaxies, we calculate the maximum redshift at which each source in the *local sample* would still be bright enough to appear in the 70 μm survey (Fig. 3, lower panel). As expected, the types of sources that make

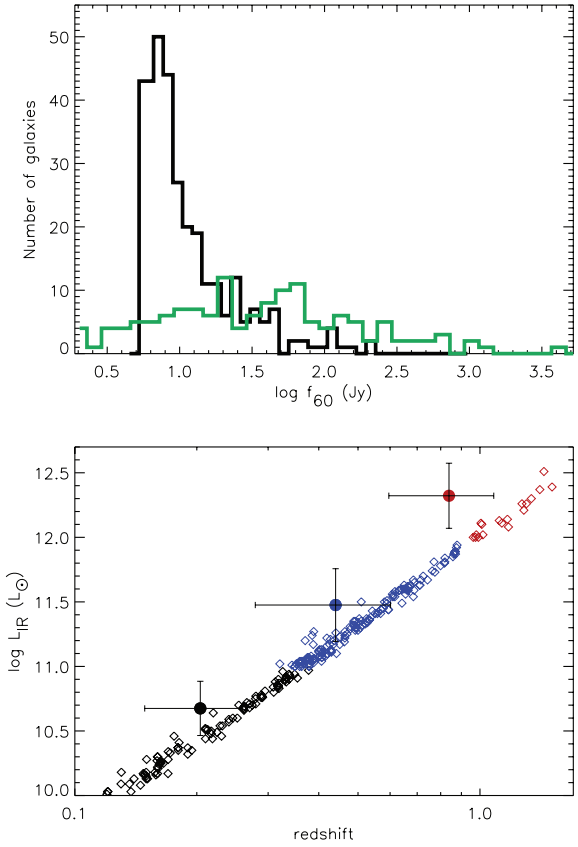

Figure 3. Top panel: the distribution in 60 μm flux density for the *local sample* (black histogram), compared with the distribution that the *70 μm sample* would have if it were at the average redshift of the local sample ($z \sim 0.012$; ∼50 Mpc) (green histogram). Note that apart from a few low-luminosity SBs ($L < 5 \times 10^{10}\,{\rm L}_{\odot}$), the 70 μm sample would be easily detectable within the 5.24 Jy *IRAS* flux density limit. Lower panel: total infrared luminosity plotted as a function of the maximum redshift at which the types of sources that form part of the *local sample* would be detectable within the 70 μm 10 mJy flux density limit – SBs in black, LIRGs in blue and ULIRGs in red. Comparing with the average $L_{\rm IR}$ and redshift for each luminosity class of the *70 μm sample* (filled circles) reveals that the 70 μm selection is quite sensitive to the LIRGs and ULIRGs of the *local sample*; at the high-luminosity end, the sources in the *local sample* can be detected to higher redshifts than the average redshift of the 70 μm galaxies.

up the *local sample* are easily recoverable at $f_{70} > 10$ mJy. In fact, at the high-luminosity end ($\log L_{\rm IR} \gtrsim 11.5$), the sources in the *local sample* are detectable to higher redshifts than the average redshift of the galaxies in the *70 μm sample*. The fact that the entire range of template matches for $L > 5 \times 10^{10}\,{\rm L}_{\odot}$ sources in both samples is detectable with the flux density limits of the *Spitzer*/MIPS, and *IRAS* surveys confirm that the samples are well-matched and that our results and conclusions (Sections 4 and 5) are not affected by the initial selection.

The final point to address is the dependency of the IR luminosity and position of SED peak on the absolute value of the 160 μm flux density. Our detection levels are at least 5σ at 70 μm and typically 4–5σ at 160 μm, so to simulate combined uncertainties we evaluate the effects of a 30 per cent change in f_{160} for all objects in the *70 μm sample*. We find that the change in luminosity does not exceed 0.2 dex and the average peak wavelength shift is less than 10 μm, well within the typical uncertainty (see Section 4.2). This confirms

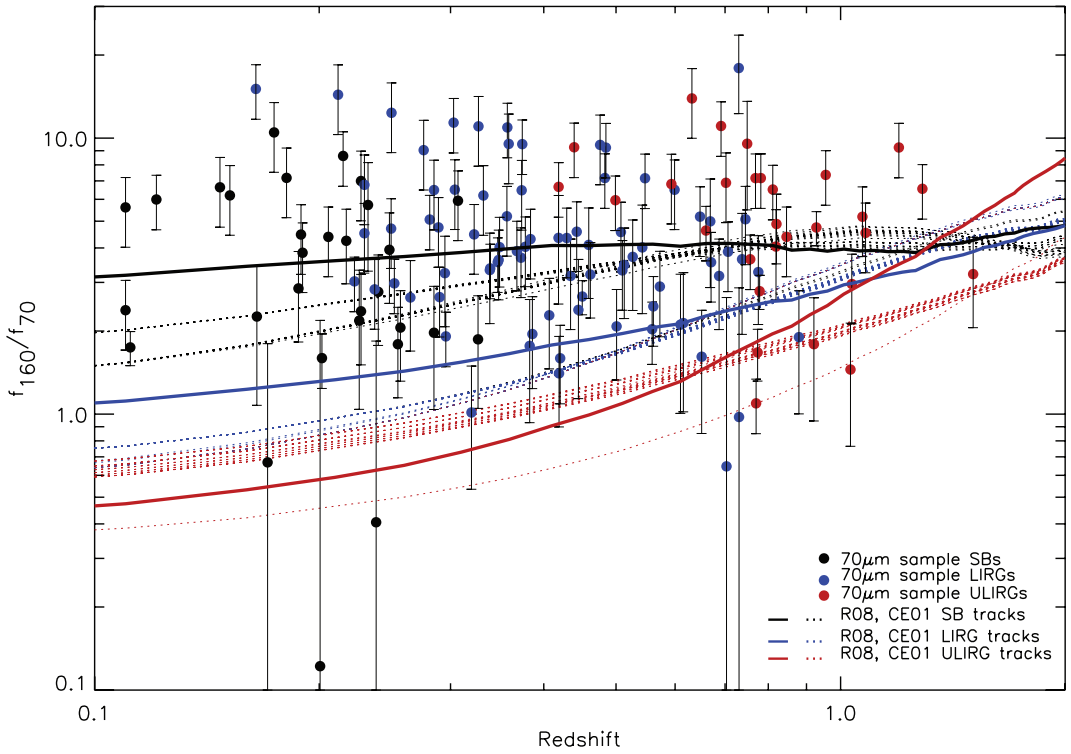

Figure 4. The 160/70 μm flux density ratio versus redshift for the SBs, LIRGs and ULIRGs of the *70 μm sample* (filled circles). The dotted line tracks are the CE01 templates and the solid line tracks are the Rieke et al. (2009) templates with luminosities of log $L_{\rm IR} = 10, 11, 12$. All templates have been convolved with the MIPS 70 and 160 μm filter response curves, since MIPS photometry is calculated from the integrated flux in each band and is therefore not strictly monochromatic. The colour coding for both data points and tracks is the same: black for SBs, blue for LIRGs and red for ULIRGs. The errors have been estimated by combining calibration, photometric and statistical uncertainties. Note the large scatter in f_{160}/f_{70} spanning almost an order of magnitude within each luminosity class. Moreover, the f_{160}/f_{70} values for many 70 μm detected LIRGs and ULIRGs are offset by at least a factor of 2 and up to 10 in extreme cases from local tracks of the same luminosity, suggesting that these sources are on average colder than their local counterparts.

that the absolute value of f_{160} does not drive our estimates for $\lambda_{\rm peak}$ and $L_{\rm IR}$.

4 RESULTS

4.1 The 160/70 μm flux density ratio

As a first approach, we examine the observed f_{160}/f_{70} colours of the *70 μm sample* as a function of redshift (Fig. 4), relying on SED templates to represent the IR colours of local galaxies. Accordingly, we chose the CE01 and Rieke et al. (2009, hereafter R09) *empirical* templates, well-representative of the average properties of local galaxies, but with some key differences in the continuum slope shortwards of the peak; R09 consider their templates more accurate for high-luminosity IR galaxies, such as Arp 220, as they account for the steeper continuum slope seen in the spectra from the InfraRed Spectrograph (IRS) on *Spitzer*.

The f_{160}/f_{70} ratio directly scales with the position of the peak, a relationship which is much clearer once *K*-corrections have been applied (see S08). Here, in order to minimize assumptions, we only compare the observed f_{160}/f_{70} colour against the locally derived tracks. However, by splitting the *70 μm sample* into luminosity classes we can evaluate f_{160}/f_{70} more consistently and in a relatively narrow redshift range. The scatter in SB f_{160}/f_{70} is in broad agreement with the local SB SEDs, with a similar number of sources lying above and below the region defined by the tracks. On the contrary, the f_{160}/f_{70} for many LIRGs and ULIRGs is displaced from the local LIRG and ULIRG tracks by at least a factor of 2 and up to 10 in extreme cases. This suggests that a large fraction of these galaxies are colder than their local equivalents, as the energetic output at long wavelengths is increased relative to the short wavelengths. Overall, the f_{160}/f_{70} colour does not seem to change with redshift and, although this would be misinterpreted as a no-evolution effect, it is in fact quite the opposite. Examining the variation of f_{160}/f_{70} with redshift will invariably have a luminosity and *K*-correction bias folded into it, as at each redshift range the survey probes galaxies at different rest-frame wavelength and of different $L_{\rm IR}$. In fact, strong evolution is evident, as the high-redshift LIRGs and ULIRGs have f_{160}/f_{70} ratios comparable to those of local low-luminosity SBs as opposed to local LIRGs and ULIRGs.

4.2 The SED peak

In Fig. 5, the variation of SED peak (rest-frame wavelength) is plotted against total infrared luminosity for the *local* and *70 μm sample*. Broadly speaking, the peak represents an average temperature for the bulk of the dust. In the nearby Universe, more luminous galaxies are characterized by emission from dust at higher temperatures which shifts the SED peak to shorter wavelengths, explicitly shown in the SED peak–$L_{\rm IR}$ relationship of the *local sample* [see also Sanders & Mirabel (1996) and the peak–$L_{\rm IR}$ variation in the R09 SED templates, overplotted for comparison].

The local and high-redshift sources, especially objects that fall in the LIRG and ULIRG luminosity class, occupy almost distinct

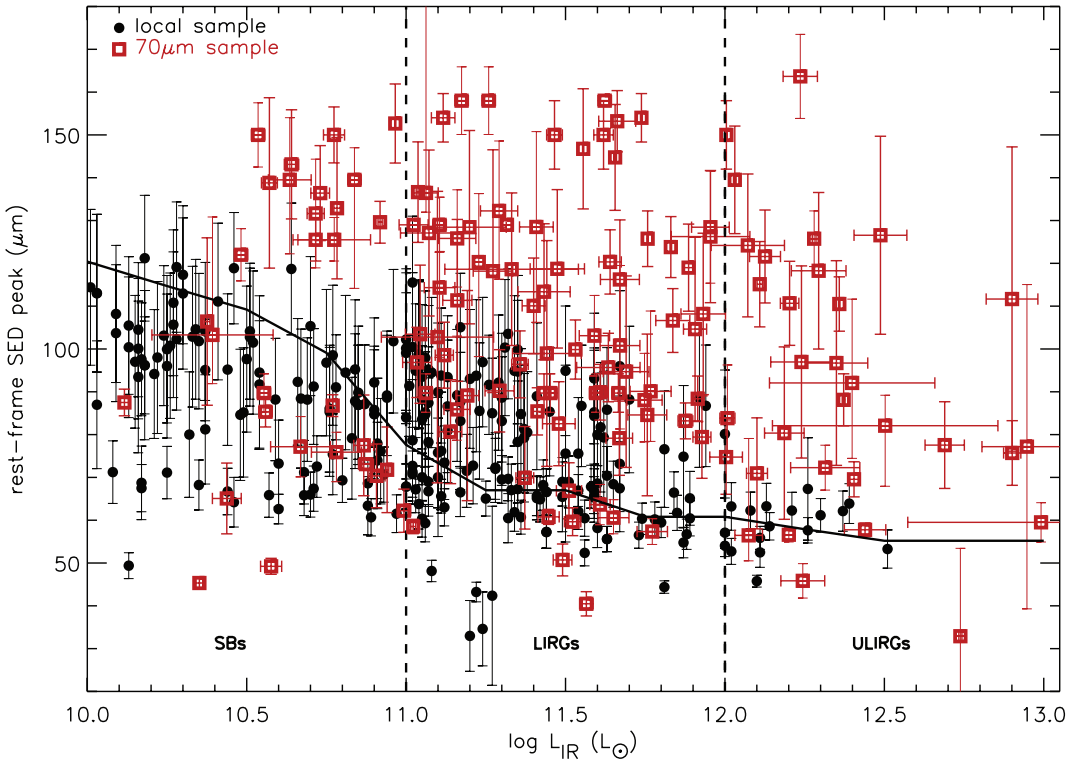

Figure 5. The relationship between SED peak and total infrared luminosity for the *local sample* (black filled circles) and *70 μm sample* (red open squares), split into three luminosity bins (SBs, LIRGs and ULIRGs), outlined by the vertical dashed lines. The solid line is the peak–L_{IR} relationship of the Rieke et al. (2009) templates. Note that for a given L_{IR}, many high-redshift galaxies have on average significantly colder SEDs that peak at longer wavelengths.

regions of this plot, signifying that for a given L_{IR}, high-redshift galaxies have on average colder SEDs that peak at longer wavelengths. Since the SED peak seems to evolve from the local to the high-redshift Universe, we might also expect it to evolve with redshift within the *70 μm sample*, i.e. from $z \sim 0.1$ to $\sim$2. However, we are unable to examine this because, as mentioned earlier, the L_{IR}–z plane is not sufficiently sampled. Under the circumstances, we rely on the more unbiased comparison between local and high-redshift sources by examining the distribution in peak wavelength separately for the three luminosity classes (Fig. 6). SBs in both samples seem to be broadly consistent, as the SB population in the *70 μm sample* is at quite a low mean redshift ($z \sim 0.2$) and cosmic evolution in the $z \sim 0$ to $\sim$0.2 interval is not expected to be prominent. However, there are a few exceptions, with some 70 μm selected SBs being colder than local equivalents, but since these sources are at low redshifts, this could be a selection effect due to the much deeper MIPS survey. As described in Section 3.2.2, this argument does not apply to the higher redshift, higher luminosity sources, and hence any differences in the types of objects picked up by the two surveys will be solely due to evolution.

Figs 5 and 6 show that, although there is some overlap in the types of objects selected in the two surveys, it seems that the SEDs of a substantial number of high-redshift LIRGs and ULIRGs peak at longer wavelengths than their local counterparts. Such a hypothesis was proposed in S08, where fitting locally derived SED templates underestimated the far-IR emission of a large fraction of high-redshift objects. Also, it seems that the galaxies in the *70 μm sample* span approximately the same range in SED peak, whatever their luminosity class, in contrast to the narrower local distribution, which notably shifts towards shorter wavelengths at higher luminosities. Although the majority of local LIRGs peak at $\sim$75 μm, with a smaller fraction at $\sim$100 μm (mean $\lambda_{peak} \sim 77$ μm), high-redshift LIRGs span a wide range in SED peak up to 160 μm, with a mean of $\sim$105 μm. This effect is even more pronounced in the ULIRGs, where the average peak in the SEDs shifts from an average local value of $\sim$60 μm to a high-redshift value of $\sim$92 μm.

4.3 Sub-mm colours

In Sections 4.1 and 4.2, we presented strong evidence that the *70 μm sample* is not simply a redshifted version of sources in the local Universe. What naturally follows is a comparison with the SubMillimetre Galaxy (SMG) population, comprising mostly of cold galaxies at high redshift. Due to the negative K-correction and sensitivity limits, SMGs discovered in blank-field surveys are mostly in the $1.5 < z < 3.5$ redshift range (e.g. Chapman et al. 2005), as the 350–850 μm wavelength range corresponds to 140–340 μm $< \lambda_{rest} <$ 78–188 μm, effectively sampling near the SED peak for a wide range of sources.

Using the SK07 fits, we predict 350 and 850 μm flux densities for the LIRGs and ULIRGs in the *70 μm sample*, with uncertainties derived from the range of best-matched templates (see Section 3.1) and plot the evolution of the f_{350}/f_{850} colour with redshift (Fig. 7). We compare with LIRG and ULIRG SMG data from Kovács et al. (2006, hereafter K06) and Coppin et al. (2008) (hereafter C08). Also plotted are the R09 tracks, to represent the local IR galaxies. As the LIRGs in the *70 μm sample* are at an average redshift of 0.4, we predict the sub-mm flux densities they would have if their redshifts were increased by 0.7 and 1.5, in order to bring them to a similar redshift range as the K06 and C08 LIRGs (top panel). Similarly,

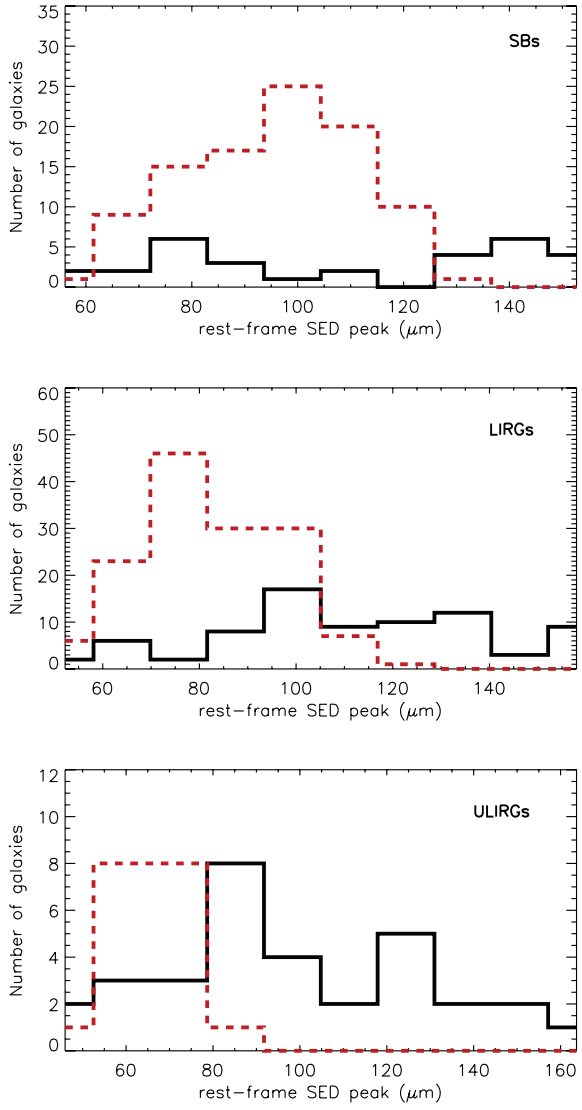

Figure 6. The distribution in SED peak for the three main luminosity classes (SBs, LIRGs and ULIRGs). The dotted red line represents the *local sample* and the solid black line represents the *70 μm sample*. Although there is overlap in the distributions, a significant fraction of high-redshift LIRGs and ULIRGs peak at longer wavelengths than the local galaxies of the same luminosity.

we calculate what sub-mm flux densities we would expect for the ULIRGs (average $z \sim 0.8$) if their redshift were increased by 1.3 and 2 (lower panel).

The majority of K06 and C08 LIRGs and ULIRGs fall below the corresponding R09 tracks, implying a lower f_{350}/f_{850} ratio; for a given $L_{\rm IR}$, sources with lower f_{350}/f_{850} are colder, as there is a shift in far-IR emission, with more flux coming out at longer wavelengths. A large number of sources from the *70 μm sample* have similarly low f_{350}/f_{850}, again mostly below what is denoted by the R09 tracks, indicative of more cold dust emission, compared to what is seen locally. The agreement in f_{350}/f_{850} between the SMGs and MIPS sources is a key result; it strongly suggests that the galaxies we detect at 70 μm are the $z < 1$ equivalents of the cold $z > 1$ sources detected in sub-mm surveys.

5 DISCUSSION

5.1 Cold galaxies at $z \lesssim 1$

We find evidence for evolution in the dust/star formation properties with redshift, initially apparent through the f_{160}/f_{70} colour and further quantified by the rest-frame wavelength of the SED peak. More specifically, we show that a population of LIRGs and ULIRGs at $0.1 < z < 2$ appears to have a cold-dust-associated far-IR excess not seen locally. Although we do identify many sources consistent with the kind of objects detected in the local Universe, such as the well-studied M82 and Arp 220 types, our results establish a shift in the rest-frame far-IR SEDs of high-redshift sources towards longer wavelengths. A simple description for this is that the shapes of the far-IR SEDs of many high-redshift sources may resemble more closely those of lower-luminosity galaxies locally.

The strong cold component identified in many of our 70 μm objects must relate closely to conditions in the ISM, as it represents an increase in far-IR/sub-mm flux compared to local galaxies and hence must represent a change in dust properties and/or star formation efficiency. For a given total infrared luminosity, sources that are described by colder SEDs may consequently be characterized by larger dust masses and/or higher dust opacity, an increase in grain emissivity or a combination of these. Another possibility is a change in the dust distribution, where a typical high-z LIRG/ULIRG may not be similar in structure to the strongly nuclear-concentrated local examples; instead, the dust could be distributed over kpc scales, consistent with measurements of their extent in CO (e.g. Tacconi et al. 2006; Iono et al. 2009).

Hints for evolution have also emerged through other studies of high redshift, IR-selected sources. For example, Rowan-Robinson et al. (2004, 2005) report results from the European Large Area *ISO* Survey (ELAIS) and the Spitzer Wide-area InfraRed Survey (SWIRE), which indicate that many IR-luminous galaxies in the 0.15–0.5 redshift range are best fitted with cool cirrus models. Examination of IR SEDs for $z > 0.5$ ULIRGs has revealed a higher cool to hot dust ratio than what is seen locally (Marcillac et al. 2006; Brand et al. 2008; Chakrabarti & McKee 2008). Sajina et al. (2006, 2008) present results based on mid- and far-IR selected samples, which suggest that their sources are better described by cooler temperatures and high far/mid-IR ratios in contrast to local ULIRGs. Le Floc'h et al. (2005) find that ISOCAM-detected LIRGS at a median redshift of $z \sim 0.7$ are characterized by half solar metallicities which could point to the IR SEDs being different from those of local LIRGs. This behaviour is an interesting complement to the evidence for evolution from mid-infrared spectroscopy and particularly the characteristics of Polycyclic Aromatic Hydrocarbon (PAH) features. The aromatic bands in high-redshift galaxies are found to be similar in prominence and profile to the aromatic bands in local galaxies of lower luminosity (e.g. Farrah et al. 2008; Pope et al. 2008), an important result as the PAH feature strengths in local galaxies are strongly correlated with emission from cold dust (Haas, Klaas & Bianchi 2002; Bendo et al. 2008).

Predictions from several studies are also in agreement with the mounting evidence that the ISM, star formation efficiency and dust properties of many high-redshift infrared galaxies significantly diverge from those in the local universe. Chemical evolution models (Calzetti & Heckman 1999; Pei, Fall & Hauser 1999) predict a lower contribution in the UV SFR density and an increase in the average A_V by a factor of 2–3 at $z \sim 1$–2, an outcome also supported by observations in Efstathiou & Rowan-Robinson (2003) and Le Floc'h et al. (2005). Le Floc'h et al. (2005) find a much stronger evolution

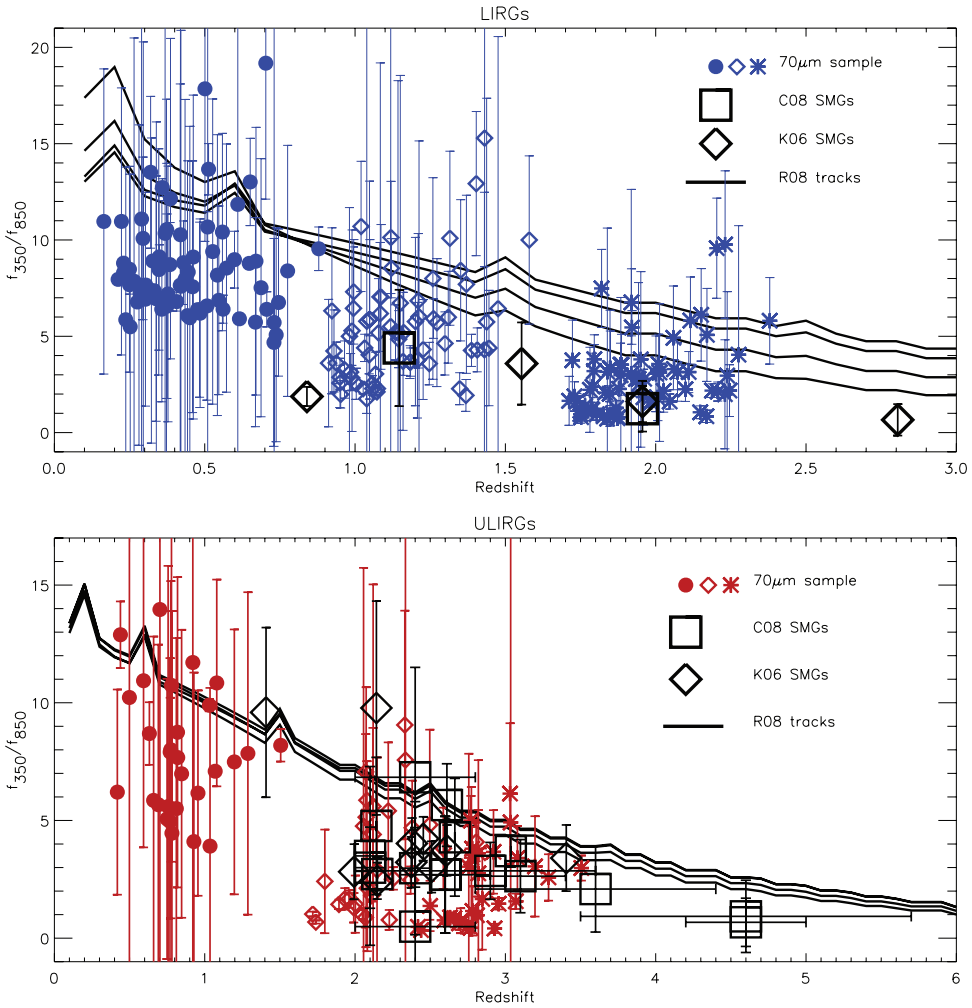

Figure 7. Plot of the f_{350}/f_{850} ratio versus redshift for LIRGs (top panel) and ULIRGs (lower panel). For reference the R09 tracks are also included (solid black curves). The flux density ratios corresponding to the *70 μm sample* are predicted using the SK07 models. Top panel: R09 LIRG tracks of log $L_{\rm IR} = 11$, 11.25, 11.5, 11.75, all LIRG SMGs from K06 (large black diamonds) and C08 (large black squares), all LIRGs in our sample at the original redshift z (blue filled circles), at a redshift z+0.7 (blue open diamonds) and at a redshift z+1.5 (blue asterisks) – the change in redshift enables a comparison with the K06 and C08 LIRGs. Lower panel: R09 ULIRG tracks of log $L_{\rm IR} = 12$, 12.25, 12.5, 12.75, all ULIRG SMGs from K06 (large black diamonds) and C08 (large black squares), the ULIRGs in our sample at the original redshift z (red filled circles), at a redshift z+1.3 (red open diamonds) and at a redshift z+2 (red asterisks) – again the redshift change brings the 70 μm detected ULIRGs to the redshift range of the K06 and C08 ULIRGs. The horizontal error bars denote errors on photometric redshifts in the C08 sample. The vertical error bars for the *70 μm sample* stem from the range of templates used to calculate f_{350}/f_{850} (see Section 3.1). Note that for a few SMGs, the uncertainty in $L_{\rm IR}$ could shift them to a higher luminosity class as some are very close to the upper luminosity limit. However, this does not alter the strong agreement in f_{350}/f_{850} colour between SMGs and the 70 μm sources, implying that we are detecting the lower redshift analogues of sub-mm galaxies.

in the infrared comoving energy density than in the UV over the same redshift range, evidence that dust reprocessing of optical light is more efficient at high redshift, but also tying in with an increase in star formation efficiency (SFR per unit cold gas mass) (Somerville, Primack & Faber 2001).

The observations and results outlined above are likely to have considerable impact in accurately modelling the far-IR and sub-mm background, as well as pinpointing the evolution in the infrared luminosity function, where the cold SED component may play a more significant role than previously thought. We expect that cold galaxies such as those we identify here will be discovered in abundance by the *Herschel Space Observatory* (Pilbratt et al. 2004). The capabilities of Herschel's Spectral and Photometric Imaging Receiver (SPIRE; Griffin et al. 2007) and Photodetector Array Camera (PACS; Poglitsch et al. 2008) will provide detailed measurements in the 60–700 μm region. This will allow accurate mapping of previously unexplored territories such as the nature of the main contributors to the cosmic infrared background and ISM properties at high redshift (Harwit 2004). The question as to whether a large fraction of IR-luminous galaxies at high redshift are cold will explicitly be answered since the SED peak will be entirely defined at least up to redshift $z \sim 3$, enabling precise temperature measurements. In addition, with *Herchel*'s capabilities the nature and properties of dust at high redshift and its evolution through cosmic time will be accurately traced.

5.2 The sub-mm/IR connection

SMGs, which are predominantly in the ULIRG and HyLIRG regime, are well-established as the most dust-rich galaxies in the Universe. Comparisons between the SEDs of SMGs and those of local and lower-redshift ($z < 1.5$) populations are therefore essential

in the context of galaxy evolution, particularly evident when modelling the behaviour of the IR and sub-mm source counts, which necessarily require the assumption of a SED shape. If SMGs are the high-redshift analogues of local warm IR galaxies, the high sub-mm counts on the faint end (with the limits of present surveys) could only be reproduced by evoking strong evolution well beyond $z \sim 3$–4, as a warm SED moves the peak to shorter wavelengths, reducing the sub-mm flux for a given $L_{\rm IR}$. This goes against the predictions of hierarchical galaxy formation models which anticipate a downturn in space density of IR-luminous sources with SFRs $> 100\,{\rm M}_{\odot}\,{\rm yr}^{-1}$ by $z \sim 3$–4. Instead, if sub-mm emission arises from a significantly cooler SED, sub-mm counts could be fit with galaxies of more moderate SFRs (Kaviani, Haehnelt & Kauffmann 2003). Predictions by Efstathiou et al. (2000), Rowan-Robinson (2001) and Efstathiou & Rowan-Robinson (2003) also support this argument, suggesting that sub-mm emission in high-redshift galaxies could predominantly arise from cold dust, proposing that the quiescent cirrus component undergoes the same strong luminosity evolution as the SB component.

Up to now, studies of SMG SEDs converge on the idea that they are predominantly fit by cooler cirrus SED templates (e.g. by Chapman et al. 2005; Pope et al. 2006; Clements et al. 2008; K06; C08). Sub-mm studies of high-redshift ULIRGs and HyLIRGs have shown that their intrinsic dust temperatures are distributed around a mean of $T \sim 35$ K (Chapman et al. 2005; Pope et al. 2006; K06; C08). Huynh et al. (2007b) report very low typical dust temperatures ($T = 21$–33 K) for a sample of $L > 5 \times 10^{11}$ low-z SMGs. Interestingly, this corresponds to the range in temperatures seen in the local SBs and LIRGs described in D00, and it is in contrast to the higher temperatures observed in local ULIRGs – the Farrah et al. (2003) local ULIRG sample is fit by $T \sim 42$ K; see also Klaas et al. (1997) and Soifer et al. (1984) where the SEDs of Arp 220 and NGC 6240 are fit by modified blackbodies of temperature 47 and 42 K, respectively. Note that even if sub-mm studies preferentially detect cold sources (e.g. Blain et al. 2004), many of these have total infrared luminosities comparable to the most energetic local galaxies, supporting the above evidence that a large number of high-redshift IR-luminous objects are colder than their local analogues. In fact, the same conclusions are reached by Sajina et al. (2008) for a sample of high-redshift mid-IR-selected sources, showing that this is not simply an artefact of the sub-mm selection.

Our results have established a connection between the far-IR and sub-mm, showing that high-redshift SMGs likely share similar properties with the lower redshift galaxies selected in *Spitzer*/MIPS surveys. We find that the predicted sub-mm colours for the 70 μm detected LIRGs and ULIRGs when redshifted to the $1.5 < z < 3.5$ range trace the same parameter space as the actual colours of sub-mm-detected sources in the same luminosity and redshift range. This suggests that we have identified the missing link between SCUBA and *Spitzer*/MIPS galaxies, i.e. a population at intermediate redshift ($z \sim 1$), detected by *Spitzer* but with the properties commonly seen in SCUBA galaxies.

6 CONCLUSIONS

We have examined the properties of a large sample of $0.1 < z < 2$ IR-luminous sources selected at 70 μm, corresponding to rest frame 23–63 μm, a selection which should strongly favour star-forming galaxies. Using available photometry in the 8–160 μm range, we fit the SK07 dust templates in order to calculate the total infrared luminosity and rest-frame wavelength of the SED peak, finding the former to be mainly in the 10^{10}–$10^{14}\,{\rm L}_{\odot}$ range and the latter at an average of ∼105 μm for the LIRGs and ∼92 μm for the ULIRGs. As the main aim of this study is to compare our results with local sources of equivalent luminosity, we use data from the local *IRAS* Bright Galaxy Sample, again fitting the photometry with the SK07 models. The locally derived SED templates of CE01 and R09 are also used as an additional comparative tool. We pay particular attention to any sources of bias that could affect our results and find nothing that could potentially predispose the outcome of our analysis.

Our major findings are as follows.

(i) By examining the f_{160}/f_{70} colour of the *70 μm sample*, we find that a large fraction of LIRGs and ULIRGs have higher f_{160}/f_{70} than what is defined by the empirical CE01 and R09 local galaxy SEDs, by at least a factor of 2 and up to 10 in extreme cases. As the f_{160}/f_{70} continuum slope is directly related to the position of the SED peak wavelength, non-trivial differences between local and high-redshift IR populations are implied.

(ii) For a given total infrared luminosity, a large fraction of the LIRG and ULIRG SEDs in the *70 μm sample* peak at wavelengths longer than 90 μm, indicative of a significant cold-dust-associated far-IR excess not detected in local sources of comparable luminosity. This behaviour is directly linked to the evolution in dust and/or star formation properties from the local to the high-redshift Universe.

(iii) We predict the f_{350}/f_{850} colours that the 70 μm selected LIRGs and ULIRGs would have if found at the average redshift of SMG populations ($1 < z < 3$) and find that they are on average equivalent to the observed SMG colours. This result suggests that we have potentially identified the $z < 1$ equivalents of the cold $z > 1$ sources discovered in blank-field sub-mm surveys.

The strong evidence that we present here drives the answer to the question that we defined at the start, i.e. whether there is a substantial number of infrared galaxies at high redshift with properties divergent from those of their local counterparts, to be yes. More specifically, our results have shown that these sources are colder rather than warmer. The emergent conclusion is that the evolution of the IR-luminous population with redshift is towards a larger dust mass or higher dust opacity and emissivity, a more extended dust distribution, higher star formation efficiency or a combination of all. The imminent *Herschel* observational programmes will be key in identifying and disentangling the main processes responsible.

ACKNOWLEDGMENTS

This work is based on observations made with the *Spitzer Space Telescope*, operated by the Jet Propulsion Laboratory, California Institute of Technology, under NASA contract 1407 and partially supported by JPL/Caltech contract 1255094 to the University of Arizona. KC is grateful for STFC fellowship support. Special thanks to David Alexander for insightful discussions.

REFERENCES

Bavouzet N., Dole H., Le Floc'h E., Caputi K. I., Lagache G., Kochanek C. S., 2008, A&A, 479, 83
Bendo G. J. et al., 2008, MNRAS, 389, 629
Blain A. W., Chapman S. C., Smail I., Ivison R., 2004, ApJ, 611, 52
Bolzonella M., Miralles J.-M., Pelló R., 2000, A&A, 363, 476
Brand K. et al., 2006, ApJ, 644, 143
Brand K. et al., 2008, ApJ, 673, 119
Brinchmann J., Ellis R. S., 2000, ApJ, 536, L77
Bundy K. et al., 2006, ApJ, 651, 120
Calzetti D., Heckman T. M., 1999, ApJ, 519, 27

Chakrabarti S., McKee C. F., 2008, ApJ, 683, 693
Chapman S. C., Blain A. W., Smail I., Ivison R. J., 2005, ApJ, 622, 772
Chary R., Elbaz D., 2001, ApJ, 556, 562 (CE01)
Chary R. et al., 2004, ApJS, 154, 80
Clements D. L. et al., 2008, MNRAS, 387, 247
Cole S., Lacey C. G., Baugh C. M., Frenk C. S., 2000, MNRAS, 319, 168
Coppin K. et al., 2008, MNRAS, 384, 1597 (C08)
Dale D. A., Helou G., 2002, ApJ, 576, 159
Dale D. A. et al., 2005, ApJ, 633, 857
Davis M. et al., 2003, Proc. SPIE, 4834, 161
Davis M. et al., 2007, ApJ, 660, L1
de Grijp M. H. K., Miley G. K., Lub J., de Jong T., 1985, Nat, 314, 240
Desai V. et al., 2008, ApJ, 679, 1204
Dole H., Lagache G., Puget J.-L., 2003, ApJ, 585, 617
Dole H. et al., 2004, ApJS, 154, 87
Dole H. et al., 2006, A&A, 451, 417
Dunne L., Eales S. A., 2001, MNRAS, 327, 697 (DE01)
Dunne L., Eales S., Edmunds M., Ivison R., Alexander P., Clements D. L., 2000, MNRAS, 315, 115 (D00)
Efstathiou A., Rowan-Robinson M., 1990, MNRAS, 245, 275
Efstathiou A., Rowan-Robinson M., 1995, MNRAS, 273, 649
Efstathiou A., Rowan-Robinson M., 2003, MNRAS, 343, 322
Efstathiou A. et al., 2000, MNRAS, 319, 1169
Farrah D., Afonso J., Efstathiou A., Rowan-Robinson M., Fox M., Clements D., 2003, MNRAS, 343, 585
Farrah D., Surace J. A., Veilleux S., Sanders D. B., Vacca W. D., 2005, ApJ, 626, 70
Farrah D. et al., 2008, ApJ, 677, 957
Franceschini A. et al., 2003, A&A, 403, 501
Frayer D. T. et al., 2006a, AJ, 131, 250
Frayer D. T. et al., 2006b, ApJ, 647, L9
Frayer D. T. et al., 2009, AJ, submitted (arXiv:0902.3273)
Genzel R. et al., 1998, ApJ, 498, 579
Gorjian V., Wright E. L., Chary R. R., 1999, BAAS, 31, 1394
Granato G. L., Danese L., 1994, MNRAS, 268, 235
Granato G. L., Lacey C. G., Silva L., Bressan A., Baugh C. M., Cole S., Frenk C. S., 2000, ApJ, 542, 710
Griffin M. et al., 2007, Adv. Space Res., 40, 612
Haas M., Klaas U., Bianchi S., 2002, A&A, 385, 23
Harwit M., 2004, Adv. Space Res., 34, 568
Houck J. R. et al., 2005, ApJ, 622, L105
Huynh M. T., Frayer D. T., Mobasher B., Dickinson M., Chary R.-R., Morrison G., 2007a, ApJ, 667, L9
Huynh M. T., Pope A., Frayer D. T., Scott D., 2007b, ApJ, 659, 305
Iono D. et al., 2009, ApJ, 695, 1537
Kaviani A., Haehnelt M. G., Kauffmann G., 2003, MNRAS, 340, 739
Kennicutt R. C. Jr, et al., 2003, PASP, 115, 928
Klaas U., Haas M., Heinrichsen I., Schulz B., 1997, A&A, 325, L21
Klaas U. et al., 2001, A&A, 379, 823
Kovács A., Chapman S. C., Dowell C. D., Blain A. W., Ivison R. J., Smail I., Phillips T. G., 2006, ApJ, 650, 592 (K06)
Lagache G., Puget J.-L., Dole H., 2005, ARA&A, 43, 727
Le Floc'h E. et al., 2004, ApJS, 154, 170
Le Floc'h E. et al., 2005, ApJ, 632, 169
Lonsdale C. J. et al., 2003, PASP, 115, 897
Lonsdale C. J. et al., 2004, ApJS, 154, 54
Low F. J., Rieke G. H., Gehrz R. D., 2007, ARA&A, 45, 43
Lu N. et al., 2003, ApJ, 588, 199
Makovoz D., Marleau F. R., 2005, PASP, 117, 1113
Marcillac D., Elbaz D., Chary R. R., Dickinson M., Galliano F., Morrison G., 2006, A&A, 451, 57
Marleau F. R. et al., 2004, ApJS, 154, 66
Miley G. K., Neugebauer G., Soifer B. T., 1985, ApJ, 293, L11
Murphy T. W. Jr., Armus L., Matthews K., Soifer B. T., Mazzarella J. M., Shupe D. L., Strauss M. A., Neugebauer G., 1996, AJ, 111, 1025
Papovich C. et al., 2007, ApJ, 668, 45
Pei Y. C., Fall S. M., Hauser M. G., 1999, ApJ, 522, 604
Pilbratt G. L., Prusti T., Heras A. M., Leeks S., Marston A. P., Vavrek R., 2004, BAAS, 36, 813
Poglitsch A. et al., 2008, Proc. SPIE, 7010, 3
Pope A. et al., 2006, MNRAS, 370, 1185
Pope A. et al., 2008, ApJ, 675, 1171
Rieke G. H. et al., 2004, ApJS, 154, 25
Rieke G. H., Alonso-Herrero A., Weiner B. J., Pérez-González P. G., Blaylock M., Donley J. L., Marcillac D., 2009, ApJ, 692, 556
Rowan-Robinson M., 2001, ApJ, 549, 745
Rowan-Robinson M. et al., 2004, MNRAS, 351, 1290
Rowan-Robinson M. et al., 2005, AJ, 129, 1183
Rowan-Robinson M. et al., 2008, MNRAS, 386, 697
Sajina A., Scott D., Dennefeld M., Dole H., Lacy M., Lagache G., 2006, MNRAS, 369, 939
Sajina A. et al., 2008, ApJ, 683, 659
Sanders D. B., Mirabel I. F., 1996, ARA&A, 34, 749
Sanders D. B., Scoville N. Z., Soifer B. T., Young J. S., Danielson G. E., 1987, ApJ, 312, 5
Sanders D. B., Mazzarella J. M., Kim D.-C., Surace J. A., Soifer B. T., 2003, AJ, 126, 1607 (S03)
Seymour N. et al., 2008, MNRAS, 386, 1695
Seymour N., Huynh M., Dwelly T., Symeonidis M., Hopkins A., McHardy I. M., Page M., Rieke G., 2009, MNRAS, in press (arXiv:0906.1817)
Siebenmorgen R., Krügel E., 2007, A&A, 461, 445 (SK07)
Siebenmorgen R., Krügel E., Laureijs R. J., 2001, A&A, 377, 735
Silva L., Granato G. L., Bressan A., Danese L., 1998, ApJ, 509, 103
Soifer B. T. et al., 1984, ApJ, 283, L1
Soifer B. T., Sanders D. B., Neugebauer G., Danielson G. E., Lonsdale C. J., Madore B. F., Persson S. E., 1986, ApJ, 303, 41
Soifer B. T., Boehmer L., Neugebauer G., Sanders D. B., 1989, AJ, 98, 766
Somerville R. S., Primack J. R., Faber S. M., 2001, MNRAS, 320, 504
Spergel D. N. et al., 2003, ApJS, 148, 175
Stanev T., Franceschini A., 1998, ApJ, 494, L159
Symeonidis M. et al., 2007, ApJ, 660, L73
Symeonidis M., Willner S. P., Rigopoulou D., Huang J.-S., Fazio G. G., Jarvis M. J., 2008, MNRAS, 385, 1015 (S08)
Tacconi L. J., Genzel R., Lutz D., Rigopoulou D., Baker A. J., Iserlohe C., Tecza M., 2002, ApJ, 580, 73
Tacconi L. J. et al., 2006, ApJ, 640, 228
Veilleux S., Sanders D. B., Kim D.-C., 1997, ApJ, 484, 92
Verma A., Charmandaris V., Klaas U., Lutz D., Haas M., 2005, Space Sci. Rev., 119, 355
Wang J. L., Xia X. Y., Mao S., Cao C., Wu H., Deng Z. G., 2006, ApJ, 649, 722
Werner M. W. et al., 2004, ApJS, 154, 1
Yan L. et al., 2004, ApJS, 154, 60
Zheng X. Z., Dole H., Bell E. F., Le Floc'h E., Rieke G. H., Rix H.-W., Schiminovich D., 2007, ApJ, 670, 301

This paper has been typeset from a TEX/LATEX file prepared by the author.